MNRAS Advance Access published May 20, 2016

Stability analysis of the *Gravito-Electrostatic Sheath*-based solar plasma equilibrium

P. K. Karmakar,[1]⋆ H. P. Goutam,[1] M. Lal[2] and C. B. Dwivedi[3]
[1] *Department of Physics, Tezpur University, Napaam-784028, Tezpur, Assam, Bharat (India)*
[2] *Dr. K. S. Krishnan Geomagnetic Research Laboratory, IIG, Leelapur road, Allahabad-211019, Uttar Pradesh, Bharat (India)*
[3] *Ved-Vijnanam Pravartanam Samitihi, Village- Jagatpur, P.O.- Kailideeh (Via Suwansa), PIN-230306, District- Pratapgarh (Awadh), Uttar Pradesh, Bharat (India)*

ABSTRACT

We present approximate solutions of non-local linear perturbational analysis for discussing the stability properties of the Gravito-Electrostatic Sheath (GES)-based solar plasma equilibrium, which is indeed non-uniform on both the bounded and unbounded scales. The relevant physical variables undergoing perturbations are the self-solar gravity, electrostatic potential and plasma flow along with plasma population density. We methodologically derive linear dispersion relation for the GES fluctuations, and solve it numerically to identify and characterize the existent possible natural normal modes. Three distinct natural normal modes are identified and named as the *GES-oscillator mode*, *GES-wave mode* and usual (classical) *p-mode*. In the solar wind plasma, only the p-mode survives. These modes are found to be linearly unstable in wide-range of the Jeans-normalized wavenumber, k. The local plane-wave approximation marginally limits the validity or reliability of the obtained results in certain radial- and k-domains only. The phase and group velocities, time periods of these fluctuation modes are investigated. It is interesting to note that, the oscillation time periods of these modes are 3-10 minutes, which match exactly with those of the observed helio-seismic waves and solar surface oscillations. The proposed GES model provides a novel physical view of the waves and oscillations of the Sun from a new perspective of plasma-wall interaction physics. Due to simplified nature of the considered GES equilibrium, it is a neonatal stage to highlight its applicability in the real Sun. The proposed GES model and subsequent fluctuation analysis need further improvements to make it more realistic.

Key words: Sun: interior - Sun: oscillations - Sun: solar wind - instabilities - hydrodynamics

1 INTRODUCTION

It is well-known that the solar plasmas, including all stellar plasmas, are bounded and are confined by the self-gravitational barrier. Hence, the role of plasma and boundary-wall interaction physics and process becomes a reality which should not be ignored while studying their equilibria and stabilities. However, earlier theoretical models for the description of solar interior and exterior plasma equilibria and dynamics did not consider the boundary effects (Christensen-Dalsgaard 2002; Alerts, Christensen-Dalsgaard & Kurtz 2010; Priest 2014) as well as self-gravitational fluctuation effects (Cowling 1941). Analogous to the laboratory plasma (Chen 1984; Riemann 1991), a pre-sheath like quasi-neutral space-charge region should be formed around the solar surface boundary (SSB) over a *Jeansean* spatial extension. Motivated by the above physical situations and conceptual arguments, a novel theoretical model of the *Gravito-Electrostatic Sheath (GES)* physics was proposed by Dwivedi, Karmakar & Tripathy (2007) to give a new physical perspective to the Sun. One can get details on plasma sheath and pre-sheath formation in laboratory (Chen 1984; Riemann 1991, 1997; Deka & Dwivedi 2010; Pandey & Vladimirov 2011) and in solar wind plasmas (Pines et al. 2010) from various sources enlisted herein.

The proposed GES model predicts a quasi-hydrostatic equilibrium of the solar interior plasma (SIP) and the hydrodynamic equilibrium of the solar wind plasma (SWP). The SIP and SWP are connected at the GES-defined SSB. The GES model gives a unified picture of the sub-sonic solar *interior* origin of the SWP, in contrast with its sub-sonic *surface* origin, as predicted by Parker's model (Parker 1958). The

⋆ E-mail: pkk@tezu.ernet.in (PKK)

GES theory reproduces Parker's SWP results. In addition, it predicts the solar surface-charging (~ -120 C) and flow of high (~ -10^{12} A m^{-2}) negative net (electron-dominated) electric current across the SSB. This terminates into positive net current at about $1R_\Theta$ away from the SSB. The defined SSB is very sensitive to a minuscule imbalance in the GES forces and hence, it is very susceptible to even little fluctuations in the net force fields. These fluctuations constitute perturbations in the self-solar gravitational sheath potential (termed as gravitational wall potential), electrostatic sheath potential, plasma density and plasma flow. The fundamental importance of the solar plasma waves and oscillations lies in its ability to probe the ultra-hot solar interior structure inaccessible for direct diagnostics.

In this research contribution, we have carried out approximate linear perturbation analysis (eigenvalue treatment) of the spherically symmetric solar plasma system under the GES equilibrium to explore its stability properties. Since the bounded and unbounded solar plasma equilibria are inhomogeneous, and hence, local linear perturbation analysis is inadequate. For simplicity, we have used the local plane-wave approximation to derive the non-local linear dispersion relations (eigenvalue equations) for the travelling Fourier wave-like solutions. The derived dispersion relations are solved by numerical methods and the possible normal modes are identified and their dispersion properties are discussed. Three distinct natural normal modes, named as the *GES-oscillator*, *GES-wave* and usual electrostatic acoustic wave called as the *p-mode*, are obtained and characterized. Detailed calculations and discussions about these modes are given in the subsequent sections of the text.

Apart from the introduction as in Section 1, Section 2 deals with the description of the plasma model and the GES-equilibrium on the bounded and unbounded scales. In Section 3, non-local linear calculations are performed to derive global linear dispersion relations for the fluctuations. Numerical calculations are carried out in Section 4 with all possible information about the wave properties. Results are discussed and conclusions are finally drawn in Section 5.

2 EQUILIBRUM PLASMA DESCRIPTION AND CONFINING FORCES

The plasma of the proposed GES-model Sun consists of mainly hydrogen ions and electrons ignoring many other ionic and neutral species which are, of course, present, but in minorities (Stix 2002; Peratt 2015). The localized self-solar gravity with radial variation of its own strength plays the role of the confining wall with its maximum strength at the derived SSB. Its strength is measured in terms of the escape velocity of the ionic fluid. The localized electrostatic sheath potential suffers a major negative potential drop in the neighborhood of the outer GES-solar surface. It terminates into a maximum negative constant value at the radial location of about $1R_\Theta$ away from the defined SSB. It produces a counter acting force to the self-solar and external solar gravity both and we call it as the electrostatic sheath rebounding force. We propose it to act as the restoring force for driving the GES-oscillator and waves. At this radial location the net current becomes zero and hence, in the usual plasma sheath terminology, the corresponding spherical surface is said to be in floating condition.

According to the GES model, the radial size ($1R_\Theta$) of the spherically symmetric plasma chamber comes out to be $R_{SSB} \sim 3.5\lambda_J = 1R_\Theta = 1.08\times10^{11}$ cm, where $\lambda_J = 3.09\times10^{10}$ cm is the well-known Jeans length. It comes out to be larger than the standard solar radius, $R_{SSM} = 6.96\times10^{10}$ cm by about 40%. Also, the mass of the model GES-Sun comes out as $M_{GES} \approx 7\times10^{33}$ g, which is also larger by about four times than the standard solar mass, $M_{SSM} = 1.99\times10^{33}$ g. The population density of the GES-solar plasma, $n_i \sim 8.5\times10^{23}$ cm^{-3}, at the initial radial point is equal to the standard mean solar density ($n_0 = \rho_\Theta/m_i$) with surface value $n_\Theta \sim 3\times10^{23}$ cm^{-3}. The isothermal electron temperature of the SIP comes out to be $T_e \sim 1\times10^7$ K with isothermal ion temperature $T_i \sim 4\times10^6$ K. The SWP plasma density varies from $n_\Theta \sim 3\times10^{23}$ cm^{-3} (at the SSB) to $n_{1AU} \sim 3\times10^{11}$ cm^{-3} (at 1 A.U). The SWP electron temperature comes out to be $T_e \sim 1\times10^6$ K with ion temperature $T_i \sim 1\times10^5$ K. Consideration of proper equation of state as well as energy transport equation may definitely improve the results to compare with the real Sun. Under constant plasma temperature, the consideration of convective effect is beyond the scope of our present GES model.

We calculate the magnitudes of various forces, like-Lorentz force (F_L) for 0.1 G magnetic field, electrostatic force according to the Pannekoek-Rosseland (P-R) model (Vranjes 2011), buoyancy force and rotational force for unit angular velocity (Priest 2014; Peratt 2015). Comparing our calculations of the GES forces, we notice [Figs 1(a, b, c, d)] that the GES-based solar plasma model equilibrium is justified for magnetic field of strength $B_0 < 1$ G. In reality, we cannot ignore the magnetic field effects, which may be incorporated in the form of the Chodura magnetic presheath formalism (Chodura 1982) with proper care of the geometry. He clearly concludes that the presence of magnetic field of any arbitrary value does not affect the net potential drop between the bulk plasma and the confining wall.

2.1 SIP-equilibrium description

The basic set of normalized equations for the description of hydrodynamic equilibrium of spherically symmetric model of the GES-solar plasma on the bounded scale is reproduced from the reference (Dwivedi et al. 2007) as

Ion continuity equation:

$$\frac{d\theta}{d\xi} + \frac{1}{M}\frac{dM}{d\xi} + \frac{2}{\xi} = 0, \tag{1}$$

The third term of this equation is originating due to spherical geometry and causes the decrease of the ion density flux due to increasing surface area of the spherical surfaces at successive radial positions relative to the center. This is what we term as the "*curvature effect*" or "*geometry effect*" appearing at different places in the text.

Ion momentum equation:

$$M\frac{dM}{d\xi} = -\alpha\frac{d\theta}{d\xi} - g_s, \tag{2}$$

Reduced form of equations (2) after equation (1):

$$\left(M^2-\alpha\right)\frac{1}{M}\frac{dM}{d\xi}=\alpha\frac{2}{\xi}-g_s, \tag{3}$$

Self-solar gravity (non-rigid confining wall) equation:

$$\frac{dg_s}{d\xi}+\left(\frac{2}{\xi}\right)g_s=e^{\theta}. \tag{4}$$

Here, g_s, θ and M stand for the normalized equilibrium self-solar gravity, normalized GES-associated electrostatic sheath potential and SIP Mach number, respectively. The self-solar gravity equation describes what we term as the non-rigid (diffused) gravitational wall. Here too, the second term on the LHS of equation (4) contains curvature effect arising due to spherical geometry (non-planar influence). The standard astrophysical normalization scheme adopted here is symbolically defined with all the usual notations as

$\xi=\frac{r}{\lambda_J}$, $M=\frac{v_i}{c_S}$, $\theta=\frac{e\phi}{T_e}$, $\eta=\frac{\psi}{c_S^2}$, $c_S=\left(\frac{T_e}{m_i}\right)^{1/2}$, $\omega_J=(4\pi\rho_\Theta G)^{1/2}$, $\epsilon_T=\frac{T_i}{T_e}$, $\alpha=1+\epsilon_T$, and $g_s=\frac{d\eta}{d\xi}$.

The unnormalized notations r, v_i, ϕ, ψ represent respectively the radial coordinate, the radial component of the solar plasma velocity, the GES associated electrostatic and gravitational sheath potentials. The other notations T_e, T_i, m_i, c_S, λ_J, e, ρ_Θ, G, ω_J stand for the unnormalized electron temperature, ion temperature, ion mass, plasma sound speed, critical Jeans length, electronic charge, mean solar density, universal gravitational constant and mean Jeans frequency, respectively. Under Boltzmannian distribution of electrons, i.e., for $N_e=N_i=N=e^{\theta}$, the electron continuity equation becomes redundant. However, its role will be included in the context of charge conservation principle as discussed in the Appendix. The nonlinear pressure gradient term, $(1/N)\,dN/d\xi$, is reduced to $d\theta/d\xi$, which is appearing in equations (1)-(2).

2.1.1 *Condition for GES-boundary*

The self-solar gravity, as a physical variable, is more suitable physical quantity that defines the non-rigid gravitational wall and its strength. Keeping this fact into mind we consider the maximization of the self-solar gravity to mathematically define the SSB. The necessary condition for g_s to become maximum at some radial position, $\xi=\xi_\Theta$, for some specified value of $\theta=\theta_\Theta$ is $dg_s/d\xi|_{\xi=\xi_\Theta}=0$. Using this condition in equation (4), we find $\xi_\Theta=2g_\Theta e^{-\theta_\Theta}$. The condition of sufficiency needs $d^2g_s/d\xi^2|_{\xi=\xi_\Theta}<0$ and to derive it, we spatially differentiate equation (4) once to get

$$\frac{d^2g_s}{d\xi^2}-\left(\frac{2}{\xi^2}\right)g_s+\left(\frac{2}{\xi}\right)\frac{dg_s}{d\xi}=e^{\theta}\frac{d\theta}{d\xi}.$$

Now, using the condition of exact hydrostatic equilibrium at the surface, $|d\theta/d\xi|_{\xi=\xi_\Theta}\approx|d\eta/d\xi|_{\xi=\xi_\Theta}=(g_s)_{\xi=\xi_\Theta}$, and using $dg_s/d\xi\,|_{\xi=\xi_\Theta}=0$ into above equation, one gets

$$\frac{d^2g_s}{d\xi^2}\,|_{\xi=\xi_\Theta}=g_\Theta\left(\frac{2}{\xi^2}-e^{\theta_\Theta}\right)<0.$$

After eliminating e^{θ_Θ}, the above inequality yields $g_\Theta\xi_\Theta>1$. If we define the escape velocity as $v_\infty=\sqrt{2g_\Theta\xi_\Theta}$, it is further reduced to $v_\infty>\sqrt{2}$. This is the required condition for the existence of a localized self-gravitational sheath of the Jeans scale width. It is similar to the usual Bohm condition for the existence of plasma sheath (Riemann 1991). Solving numerically the basic set of equations (1)-(4) as an initial value problem, the boundary is found to exist at $\xi\sim3.5$ (see Fig. 6 of Karmakar & Dwivedi 2011). Existence of the subsonic electrostatic pre-sheath on the Jeans scale length with major potential drop beyond the SSB becomes a reality in the presence of negative current flowing across the SSB. In similar situation with negative current across a surface in laboratory plasmas also (Loizu, Ricci & Theiler 2011), the sub-sonic electrostatic sheath is studied.

2.1.2 *Equilibrium of GES Sun*

To understand the true nature of the SIP equilibrium, let us look into the radial profile of the net GES force ($F_{GES}=-g_s-\alpha d\theta/d\xi$) as shown in Fig. 1(a). It shows small deviation from the exact hydrostatic equilibrium due to non-zero but very small net force. Moreover, due to finite ion temperature, there is a directional change in the net force from radially inward to outward at $\xi=1.5$, i.e., $r=0.4R_\Theta$. Fig. 1(b) depicts the radial profile of the net GES potential ($V_{GES}=\eta+\alpha\theta$), which acts as a potential barrier all through the solar interior region up to the surface. Fig. 1(c) depicts the net effect of curvature or geometry and gravitational acceleration ($F_C=2\alpha/\xi-g_s$). It is seen that the curvature term in equation (3) dominates over g_s, and hence, a subsonic plasma flow with strong deceleration exists up to about $\xi=1.5$. As a result, the GES theory predicts a quasi-hydrostatic equilibrium of the SIP.

This is to emphasize further that the electric field estimated by the P-R model (Vranjes 2011) calculation comes out to be smaller than that by us, as depicted in Fig. 1(d). The estimation of current density (eq. [A4], Appendix) at the defined SSB by the GES theory, $j_{SSB}\sim10^{12}$ A m^{-2} = 1 TA m^{-2} (where, 1 T = 10^{12}, termed as 1 tera), is extremely high, which is beyond the limit of physical reality! Similarly, the corresponding magnetic field comes out to be $B_{SSB}\sim10^{21}$ G at the SSB defined by the GES model. It further increases in the SWP linearly with radial position. Despite the high B_{SSB}-values, the electrostatic potential drop between the SIP and SSB would not be influenced according to the well-known Chodura conclusion (Chodura 1982).

2.2 SWP-equilibrium description

The SWP dynamics is not affected by the self-solar gravity, because it is switched off at the defined SSB. The SSB forms a diffused transition layer, where the self-solar gravity transforms from internal (not following the *Newtonian inverse square law*) to external one, following the *inverse square law*. Here, the external solar gravity affects only the equilibrium structure of the SWP as we will see in the next subsection. The basic equilibrium governing equations for the SWP dynamics are given as

Ion momentum equation:

$$M\frac{dM}{d\xi}=-\alpha\frac{d\theta}{d\xi}-\frac{a_0}{\xi^2}. \tag{5}$$

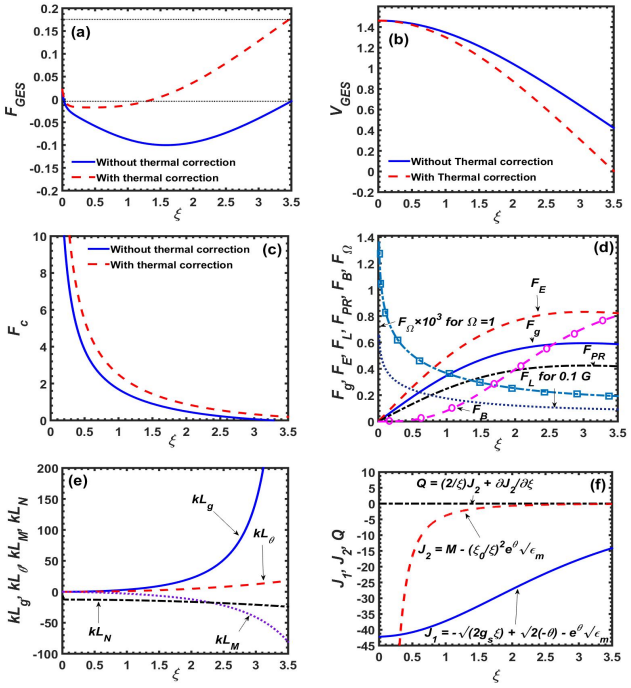

Figure 1. Profile of the normalized (a) net equilibrium GES force without thermal contribution [$F_{GES} = -(g_s + d\theta/d\xi)$, blue solid line] and with thermal contribution [$F_{GES} = -(g_s + \alpha d\theta/d\xi)$, $\alpha = (1 + \epsilon_T)$, red dashed line]; (b) net equilibrium GES potential without thermal contribution [$V_{GES} = (\eta + \theta)$, blue solid line], and with thermal contribution [$V_{GES} = (\eta + \alpha\theta)$, red dashed line]; (c) net effect of curvature and gravitational forces without thermal contribution [$F_C = (2/\xi - g_s)$, blue solid line], and with thermal contribution [$F_C = (2\alpha/\xi - g_s)$, red dashed line]; (d) gravitational force [$F_g = g_s$], electrostatic force with thermal contribution [$F_E = -\alpha d\theta/d\xi$], Lorentz force [$F_L = (\omega_{ci}/\omega_J)M$, for $B_0 = 0.1$ G], gravity-induced electrostatic force [$F_{PR} = \{(m_iT_e - m_eT_i)/m_i(T_e + T_i)\}g_s$], buoyancy force [$F_b = -(\gamma - 1)g_s^2\xi$], and Coriolis force [$F_\Omega = -(2\Omega_{rot}/\omega_J)M$, rescaled by multiplying with 10^3 for $\Omega_{rot} = 1$ rad s^{-1}]; (e) product of wave number (k) and scale-length (L) for self-solar gravity [kL_g], electrostatic potential [kL_θ], Mach number [kL_M], and population density [kL_N]; and (f) previous current density [J_1] without geometrical effects, new current density [J_2, rescaled by multiplying with 10^3] with geometrical effects, and charge-conservation parameter [$Q = (2/\xi)J_2 + \partial J_2/\partial\xi$] in the SIP with position (ξ). Different input and initial values are in the text.

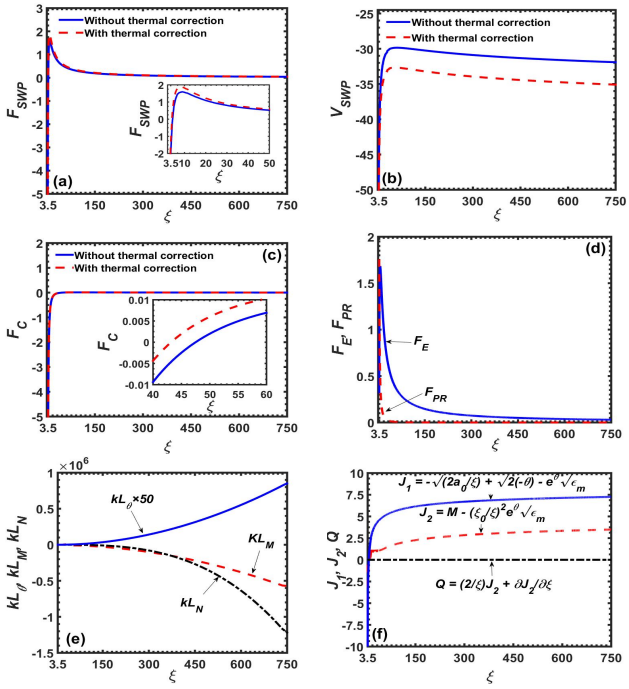

Figure 2. Profile of the normalized (a) net equilibrium force without thermal contribution [$F_{SWP} = -(\partial\theta/\partial\xi + a_0/\xi^2)$, blue solid line], and with thermal contribution [$F_{SWP} = -(\alpha\partial\theta/\partial\xi + a_0/\xi^2)$, $\alpha = (1 + \epsilon_T)$, red dashed line]; (b) net equilibrium potential without thermal contribution [$V_{SWP} = (\theta - a_0/\xi)$, blue solid line], and with thermal contribution [$V_{SWP} = (\alpha\theta - a_0/\xi)$, red dashed line]; (c) net effect of curvature and gravitational forces without thermal contribution [$F_C = (2/\xi - a_0/\xi^2)$, blue solid line], and with thermal contribution [$F_C = (2\alpha/\xi - a_0/\xi^2)$, red dashed line]; (d) electrostatic force with thermal contribution [$F_E = -\alpha\partial\theta/\partial\xi$], and gravity-induced electrostatic force [$F_{PR} = \{(m_iT_e - m_eT_i)/m_i(T_e + T_i)\}(a_0/\xi^2)$]; (e) product of wave number (k) and scale-length (L) for electrostatic potential [kL_θ], Mach number [kL_M], and population density [kL_N]; and (f) previous current density [J_1] without geometrical effects, corrected current density [J_2] with geometrical effects, and charge-conservation parameter [$Q = (2/\xi)J_2 + \partial J_2/\partial\xi$] in the SWP with position (ξ). The input and initial values used are highlighted in the text.

Ion continuity equation is the same as given by equation (1). Equations (2) and (5) can be combined to yield

$$\left(M^2 - \alpha\right)\frac{1}{M}\frac{dM}{d\xi} = \frac{2\alpha}{\xi} - \frac{a_0}{\xi^2}, \tag{6}$$

where, $a_0 = GM_\Theta/c_S^2\lambda_J$ is a normalization constant measuring the SWP temperature in the same normalization scheme.

2.2.1 Hydrodynamic equilibrium of SWP

Fig. 2(a) is plotted to depict the net GES force $\left(F_{SWP} = -\alpha d\theta/d\xi - a_0/\xi^2\right)$ acting on the SWP flow. It is clear to note that $F_{SWP} > 0$ beyond about $\xi = 5$, i.e., $r = 1.4R_\Theta$, and it goes maximum at about $\xi = 8$, i.e., $r = 2.3R_\Theta$ away from the SSB. This is the region where the SWP is accelerated from sub-sonic to sonic levels (see Fig. 4(c) of Dwivedi et al. 2007), and this is consistent with equation (5). Fig. 2(b) depicts the profile of negative net potential ($V_{SWP} = \alpha\theta - a_0/\xi$), which clearly indicates the existence of a potential well. The curvature effect $\left(F_C = 2\alpha/\xi - a_0/\xi^2\right)$, as shown in Fig. 2(c), is weaker in comparison with the external gravitational force. However, the F_C-effect becomes prominent after $\xi = 47.5$, i.e., $r \approx 14R_\Theta$, where, the SWP flow suffers transonic transformation from sonic to supersonic speeds (see Fig. 4(c) of Dwivedi et al. 2007), and this is also consistent with equation (6). Thus, the SWP equilibrium is hydrodynamic in nature with free-fall motion of the plasma on large scales of the Jeans order. This is again to emphasize that the electric field estimated by the P-R model calculation for the SWP also comes out to be smaller than that by GES model as in Fig. 2(d).

We give a schematic diagram of the GES and standard solar model (SSM) equilibria in Figs 3(a, b). Accordingly, in Figs 3(a, b), we portray schematic diagram of the Sun and

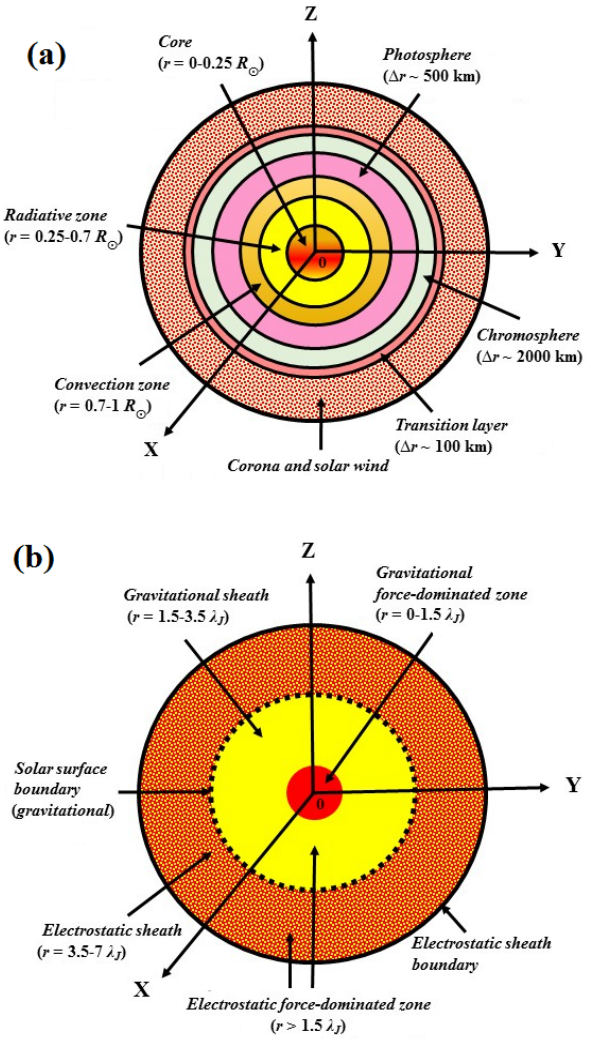

Figure 3. Schematic diagram of the Sun and its ambient atmosphere according to the (a) standard solar model (SSM), and (b) gravito-electrostatic sheath (GES) model. The solar surface in the former lies in the photosphere, named spectroscopically, after emission of most visible light from the Sun. The surface in the latter is defined by the maximization of the self-solar gravity wall strength amid exact gravito-electrostatic force balancing.

its ambient atmosphere according to the (a) SSM, and (b) GES model. According to the latter, the SSB includes excess concentric region composed jointly of the solar photosphere ($\Delta r \sim 500$ km), chromosphere ($\Delta r \sim 200$ km) and marginally, the coronal base (inner, $\Delta r \leq 1 R_\Theta$). As per the spectroscopic definition, the SSB lies in the photosphere, where the opacity becomes unity for the visible light (green, 5000 Å, at $r = 1 R_\Theta$) emission from the Sun. From Figs 3(a, b), we can notice that the SSM-Sun consists of more multiple zones as compared to the GES-Sun. We now turn over the discussions of the non-local linear perturbations and their normal mode analysis by analytical and numerical methods.

3 NON-LOCAL LINEAR WAVE ANALYSIS

3.1 GES fluctuations in SIP

The GES equilibrium for this problem has already been described. We focus our efforts to look into the perturbation part only. The set of unnormalized time-dependent equations for the quasi-neutral SIP dynamics are given as

Ion momentum equation:

$$\frac{\partial v_i}{\partial t} + v_i \frac{\partial v_i}{\partial r} = -\left(\frac{e}{m_i}\right)\frac{\partial \phi}{\partial r} - \left(\frac{T_i}{m_i}\right)\left(\frac{1}{n_i}\right)\frac{\partial n_i}{\partial r} - \frac{\partial \psi}{\partial r}, \tag{7}$$

Ion continuity equation:

$$\frac{\partial n_i}{\partial t} + \frac{1}{r^2}\frac{\partial}{\partial r}\left(n_i v_i r^2\right) = 0, \tag{8}$$

Self-solar gravity (non-rigid confining wall) equation:

$$\frac{d^2\psi}{dr^2} + \left(\frac{2}{r}\right)\frac{d\psi}{dr} = 4\pi G m_i n_i. \tag{9}$$

This is to notice that the self-solar gravitational wall equation is time-independent. This is due to the fact that the gravitational Poisson equation (eq. [9]), which defines and mimics the non-rigid stationary wall of our model consideration, is intrinsically time-independent. Now, using the normalization procedure as defined earlier along with a new notation $\tau = \omega_J t$ for the normalized time, we set out the normalized forms of equations (7)-(9) respectively as

$$\frac{\partial M}{\partial \tau} + M\frac{\partial M}{\partial \xi} = -\alpha\frac{\partial \theta}{\partial \xi} - g_s, \tag{10}$$

$$\frac{\partial \theta}{\partial \tau} + M\frac{\partial \theta}{\partial \xi} + \frac{\partial M}{\partial \xi} + \left(\frac{2}{\xi}\right)M = 0, \tag{11}$$

$$\frac{dg_s}{d\xi} + \left(\frac{2}{\xi}\right)g_s = e^{\theta}. \tag{12}$$

Now, splitting the physical variables linearly into equilibrium and fluctuation parts as defined below

$$\begin{pmatrix} M \\ \theta \\ g_s \end{pmatrix}(\xi,\tau) = \begin{pmatrix} M_0 \\ \theta_0 \\ g_{s0} \end{pmatrix}(\xi) + \begin{pmatrix} \tilde{M} \\ \tilde{\theta} \\ \tilde{g_s} \end{pmatrix}(\xi,\tau), \tag{13}$$

we linearise equations (10)-(12) respectively as

$$\frac{\partial \tilde{M}}{\partial \tau} + M_0\frac{\partial \tilde{M}}{\partial \xi} + \tilde{M}\frac{\partial M_0}{\partial \xi} = -\alpha\frac{\partial \tilde{\theta}}{\partial \xi} - \tilde{g_s}, \tag{14}$$

$$\frac{\partial \tilde{\theta}}{\partial \tau} + M_0\frac{\partial \tilde{\theta}}{\partial \xi} + \tilde{M}\frac{\partial \theta_0}{\partial \xi} + \frac{\partial \tilde{M}}{\partial \xi} + \left(\frac{2}{\xi}\right)\tilde{M} = 0, \tag{15}$$

$$\frac{d\tilde{g_s}}{d\xi} + \left(\frac{2}{\xi}\right)\tilde{g_s} = e^{\theta_0}\tilde{\theta}. \tag{16}$$

It is clear to note from equations (14)-(16) that the fluctuations are dynamically coupled with the equilibrium. As a result, quasi-linear effects, i.e., the coupling of the linear perturbations with the equilibrium have already gone into mathematical calculations and description of the linear normal modes of the GES fluctuations. Equation (16) describes the self-solar gravitational wall strength fluctuations coupled with the GES associated equilibrium electrostatic potential

and fluctuations. This is how the self-solar gravitational wall fluctuations are coupled with the enclosed plasma fluctuations through equations (14)-(15).

Now to proceed further, we would like to state that the medium is inhomogeneous, and for very short-wavelength ($kL >> 1$) [Fig. 1(e)] perturbations, a local plane-wave ($k\xi > 1$) (Priest 2014; Ostashev & Wilson 2016) approximation provides a valid first approximation as

$$\begin{pmatrix} \tilde{M} \\ \tilde{\theta} \\ \tilde{g_s} \end{pmatrix}(\xi,\tau) = \begin{pmatrix} \tilde{M}(\xi) \\ \tilde{\theta}(\xi) \\ \tilde{g_s}(\xi) \end{pmatrix} e^{-i\omega\tau + ik\xi}. \tag{17}$$

Applying the above Fourier wave-like solutions in equations (14)-(16), we deduce respectively the following set of equations describing the SIP fluctuation dynamics

$$\left[\frac{\partial}{\partial\xi} + \frac{\partial\theta_0}{\partial\xi} + \left(ik + \frac{2}{\xi}\right)\right]\tilde{M}(\xi) = i\Omega\tilde{\theta}(\xi) - M_0\frac{\partial\tilde{\theta}(\xi)}{\partial\xi}, \tag{18}$$

$$\left[M_0\frac{\partial}{\partial\xi} - i\Omega + \frac{\partial M_0}{\partial\xi}\right]\tilde{M}(\xi) = -\left[\alpha\frac{\partial\tilde{\theta}(\xi)}{\partial\xi} + i\alpha k\tilde{\theta}(\xi) + \tilde{g_s}(\xi)\right], \tag{19}$$

$$\frac{\partial\tilde{g_s}(\xi)}{\partial\xi} + ik\tilde{g_s}(\xi) + \left(\frac{2}{\xi}\right)\tilde{g_s}(\xi) = e^{\theta_0}\tilde{\theta}(\xi), \tag{20}$$

where, the variables having "0" subscripts define the equilibrium parameters and $\Omega = (\omega - kM_0)$ defines the Doppler-shifted wave frequency. Now, let us introduce an operator formalism by defining the following differential operators appearing on the LHS of equations (18)-(19) as

$$\hat{O}_1 := \frac{\partial}{\partial\xi} + \frac{\partial\theta_0}{\partial\xi} + \left(ik + \frac{2}{\xi}\right), \tag{21}$$

$$\hat{O}_2 := M_0\frac{\partial}{\partial\xi} - i\Omega + \frac{\partial M_0}{\partial\xi}. \tag{22}$$

We allow $\hat{O}_1$ to operate over equation (19) and $\hat{O}_2$ over equation (18). Under commutative property of these two operators, the resulting differential equations can be combined together to yield two distinct ordinary differential equations respectively for the evolution of $\tilde{\theta}(\xi)$ and $\tilde{M}(\xi)$ as

$$\alpha_1\frac{\partial^2\tilde{\theta}(\xi)}{\partial\xi^2} + \beta_1\frac{\partial\tilde{\theta}(\xi)}{\partial\xi} + \gamma_1\tilde{\theta}(\xi) = -\frac{\partial\tilde{g_s}(\xi)}{\partial\xi} - \delta_1\tilde{g_s}(\xi), \tag{23}$$

$$\frac{\partial M_0}{\partial\xi}\frac{\partial\tilde{M}(\xi)}{\partial\xi} + ik\frac{\partial M_0}{\partial\xi}\tilde{M}(\xi) + \frac{\partial^2 M_0}{\partial\xi^2}\tilde{M}(\xi) = M_0\frac{\partial^2\theta_0}{\partial\xi^2}\tilde{M}(\xi) - \left(\frac{2}{\xi^2}\right)M_0\tilde{M}(\xi), \tag{24}$$

where,

$$\alpha_1 = \left[\alpha - M_0^2\right],$$

$$\beta_1 = \left[2i\Omega M_0 - 2M_0\frac{\partial M_0}{\partial\xi} + i\alpha k + \alpha\frac{\partial\theta_0}{\partial\xi} + \alpha\left(ik + \frac{2}{\xi}\right)\right],$$

$$\gamma_1 = \left[-ikM_0\frac{\partial M_0}{\partial\xi} + \Omega^2 + i\Omega\frac{\partial M_0}{\partial\xi} + i\alpha k\frac{\partial\theta_0}{\partial\xi} + i\alpha k\left(ik + \frac{2}{\xi}\right)\right],$$

$$\delta_1 = \left[\frac{\partial\theta_0}{\partial\xi} + \left(ik + \frac{2}{\xi}\right)\right].$$

Equation (23) clearly shows the linear coupling of $\tilde{\theta}(\xi)$ and $\tilde{g_s}(\xi)$, whereas $\tilde{M}(\xi)$ [eq. (24)] evolves independently. It can be inferred from equation (24) that the existence of plasma flow fluctuations $\left[\tilde{M}(\xi)\right]$ is a direct consequence of non-local effects in non-planar geometric approximation. This is to note that equation (23) is a coupled differential equation and it is mathematically easy to eliminate $\tilde{\theta}(\xi)$ to derive an independent differential equation for $\tilde{g_s}(\xi)$. For this, let us first derive the following relations from equation (20)

$$\tilde{\theta}(\xi) = e^{-\theta_0}\left[\frac{\partial\tilde{g_s}(\xi)}{\partial\xi} + \left(ik + \frac{2}{\xi}\right)\tilde{g_s}(\xi)\right].$$

Let us differentiate it once to deduce

$$\frac{\partial\tilde{\theta}(\xi)}{\partial\xi} = e^{-\theta_0}\left[\frac{\partial^2\tilde{g_s}(\xi)}{\partial\xi^2} + a_{01}\frac{\partial\tilde{g_s}(\xi)}{\partial\xi} - b_{01}\tilde{g_s}(\xi)\right].$$

Let us again differentiate it further to yield

$$\frac{\partial^2\tilde{\theta}(\xi)}{\partial\xi^2} = e^{-\theta_0}\left[\frac{\partial^3\tilde{g_s}(\xi)}{\partial\xi^3} + a_{02}\frac{\partial^2\tilde{g_s}(\xi)}{\partial\xi^2} + b_{02}\frac{\partial\tilde{g_s}(\xi)}{\partial\xi} + c_{02}\tilde{g_s}(\xi)\right],$$

where, the involved coefficients in the above are

$$a_{01} = \left[\left(ik + \frac{2}{\xi}\right) - \frac{\partial\theta_0}{\partial\xi}\right],$$

$$b_{01} = \left[\left(ik + \frac{2}{\xi}\right)\frac{\partial\theta_0}{\partial\xi} + \frac{2}{\xi^2}\right],$$

$$a_{02} = \left[\left(ik + \frac{2}{\xi}\right) - 2\frac{\partial\theta_0}{\partial\xi}\right],$$

$$b_{02} = \left[-2\left(ik + \frac{2}{\xi}\right)\frac{\partial\theta_0}{\partial\xi} - \frac{4}{\xi^2} + \left(\frac{\partial\theta_0}{\partial\xi}\right)^2 - \frac{\partial^2\theta_0}{\partial\xi^2}\right],$$

$$c_{02} = \left[\left(ik + \frac{2}{\xi}\right)\left\{\left(\frac{\partial\theta_0}{\partial\xi}\right)^2 - \frac{\partial^2\theta_0}{\partial\xi^2}\right\} + \frac{4}{\xi^2}\left(\frac{\partial\theta_0}{\partial\xi} + \frac{1}{\xi}\right)\right].$$

Now, substituting $\tilde{\theta}(\xi)$ and its derivatives in equation (23), one derives the following third-order linear differential equation for describing the dispersion properties of the GES fluctuations and their amplitude variations as

$$\alpha_2\frac{\partial^3\tilde{g_s}(\xi)}{\partial\xi^3} + \beta_2\frac{\partial^2\tilde{g_s}(\xi)}{\partial\xi^2} + \gamma_2\frac{\partial\tilde{g_s}(\xi)}{\partial\xi} + \delta_2\tilde{g_s}(\xi) = 0, \tag{25}$$

where,

$$\alpha_2 = \alpha_1 = \left[\alpha - M_0^2\right],$$

$$\beta_2 = \left(ik + \frac{2}{\xi}\right)\left(2\alpha - M_0^2\right) - \left(\alpha - 2M_0^2\right)\frac{\partial\theta_0}{\partial\xi} + 2i\Omega M_0 - 2M_0\frac{\partial M_0}{\partial\xi} + ik\alpha,$$

$$\gamma_2 = \left\{-2\left(ik + \frac{2}{\xi}\right)\frac{\partial\theta_0}{\partial\xi} - \frac{4}{\xi^2} + \left(\frac{\partial\theta_0}{\partial\xi}\right)^2 - \frac{\partial^2\theta_0}{\partial\xi^2}\right\}\left(\alpha - M_0^2\right) + \left\{2i\Omega M_0 - 2M_0\frac{\partial M_0}{\partial\xi} + i\alpha k + \alpha\frac{\partial\theta_0}{\partial\xi} + \alpha\left(ik + \frac{2}{\xi}\right)\right\} \times \left\{\left(ik + \frac{2}{\xi}\right) - \frac{\partial\theta_0}{\partial\xi}\right\} + \Omega^2 - ikM_0\frac{\partial M_0}{\partial\xi} + i\Omega\frac{\partial M_0}{\partial\xi} + ik\alpha\frac{\partial\theta_0}{\partial\xi} + ik\alpha\left(ik + \frac{2}{\xi}\right) + e^{\theta_0},$$

$$\delta_2 = \left[\Omega^2 - k^2\alpha + ik\alpha\frac{\partial\theta_0}{\partial\xi} - ikM_0\frac{\partial M_0}{\partial\xi} + i\Omega\frac{\partial M_0}{\partial\xi} + \frac{2ik\alpha}{\xi}\right]\left(ik + \frac{2}{\xi}\right) + \left[\left(ik + \frac{2}{\xi}\right)\left\{\left(\frac{\partial\theta_0}{\partial\xi}\right)^2 - \frac{\partial^2\theta_0}{\partial\xi^2}\right\} + \left(\frac{4}{\xi^2}\right)\frac{\partial\theta_0}{\partial\xi} + \frac{4}{\xi^3}\right]\left(\alpha - M_0^2\right)$$

$$+\left\{\frac{\partial\theta_0}{\partial\xi}+\left(ik+\frac{2}{\xi}\right)\right\}e^{\theta_0}-\left\{\left(ik+\frac{2}{\xi}\right)\frac{\partial\theta_0}{\partial\xi}+\frac{2}{\xi^2}\right\}$$
$$\times\left\{2i\Omega M_0-2M_0\frac{\partial M_0}{\partial\xi}+i\alpha k+\alpha\frac{\partial\theta_0}{\partial\xi}+\alpha\left(ik+\frac{2}{\xi}\right)\right\}.$$

Equation (25) is the desired differential equation revealing two distinct parts. The lowest-order term, $\partial^0_\xi\tilde{g_s}(\xi)$, when equated to zero (for any arbitrarily small amplitude), yields the desired non-local linear dispersion relation (eigen-value equation). The remaining 3rd order differential equation (eigen-function equation) gives the corresponding amplitude variation. The arbitrariness in the linear local fluctuation level is now removed. Equating the lowest-order term to zero, we get the dispersion relation as

$$\left[\Omega^2-k^2\alpha+ik\alpha\frac{\partial\theta_0}{\partial\xi}-ikM_0\frac{\partial M_0}{\partial\xi}+i\Omega\frac{\partial M_0}{\partial\xi}+\frac{2ik\alpha}{\xi}\right]\left(ik+\frac{2}{\xi}\right)$$
$$+\left[\left(ik+\frac{2}{\xi}\right)\left\{\left(\frac{\partial\theta_0}{\partial\xi}\right)^2-\frac{\partial^2\theta_0}{\partial\xi^2}\right\}+\left(\frac{4}{\xi^2}\right)\frac{\partial\theta_0}{\partial\xi}+\frac{4}{\xi^3}\right]\left(\alpha-M_0^2\right)$$
$$-\left\{2i\Omega M_0-2M_0\frac{\partial M_0}{\partial\xi}+i\alpha k+\alpha\frac{\partial\theta_0}{\partial\xi}+\alpha\left(ik+\frac{2}{\xi}\right)\right\}$$
$$\times\left\{\left(ik+\frac{2}{\xi}\right)\frac{\partial\theta_0}{\partial\xi}+\frac{2}{\xi^2}\right\}+\left\{\frac{\partial\theta_0}{\partial\xi}+\left(ik+\frac{2}{\xi}\right)\right\}e^{\theta_0}=0. \quad (26)$$

The remaining differential terms in equation (25) are as

$$\alpha_2\frac{\partial^3\tilde{g_s}(\xi)}{\partial\xi^3}+\beta_2\frac{\partial^2\tilde{g_s}(\xi)}{\partial\xi^2}+\gamma_2\frac{\partial\tilde{g_s}(\xi)}{\partial\xi}=0. \quad (27)$$

The amplitude variation of the GES associated $\tilde{\theta}(\xi)$ can be estimated from equation (27), and then, substituting the obtained $\tilde{g_s}(\xi)$ in equation (20). It is noted that the mathematical approach of differential operator formalism is quite general in nature. In fact, handling the problems of wave behavior in non-uniform plasma is itself mathematically complicated. The non-uniformity in multiple variables (like, in the Sun) further complicates the mathematical treatment. However, this mathematical approach provides a simple way to derive non-local linear dispersion relation. In the absence of non-local effects in the plane-geometry approximation ($\xi\to\infty$), equation (26) is reduced to the usual Jeans mode (Jeans 1902; Pandey, Avinash & Dwivedi 1994) as

$$\Omega^2=\left(\alpha k^2-1\right). \quad (28)$$

Its numerical plots on the mode frequencies, phase velocity, group velocity and time period are given in Figs 11(a, b, c, d) to offer a known standard to compare with the corresponding numerical profiles dictated by equation (26). Details will be discussed in the next section. Now, let us go for the non-local linear analysis of the SWP fluctuations.

3.2 SWP fluctuations

The considered plasma model for our GES-SWP is the same as the SIP, but with different plasma parameters as discussed in section 2. The self-solar gravity effect is switched off and the Sun acts as an external source of the solar gravity to monitor and tailor the SWP dynamics. As earlier, we ignore magnetic field and other effects just for simplicity. The basic set of normalized coupled time-dependent equations for the SWP fluctuations is written as

Ion continuity equation:

$$\frac{\partial\theta}{\partial\tau}+M\frac{\partial\theta}{\partial\xi}+\frac{\partial M}{\partial\xi}+\left(\frac{2}{\xi}\right)M=0, \quad (29)$$

Ion momentum equation:

$$\frac{\partial M}{\partial\tau}+M\frac{\partial M}{\partial\xi}=-\alpha\frac{\partial\theta}{\partial\xi}-\frac{a_0}{\xi^2}. \quad (30)$$

These equations simply describe the flow dynamics of the radially outflowing solar plasma controlled by the external solar gravity as appearing in the second term in RHS of equation (30). Applying the same mathematical approach as adopted in the SIP, we can derive the following differential equations for the description of the SWP fluctuations as

$$\frac{\partial\tilde{\theta}}{\partial\tau}+M_0\frac{\partial\tilde{\theta}}{\partial\xi}+\tilde{M}\frac{\partial\theta_0}{\partial\xi}+\frac{\partial\tilde{M}}{\partial\xi}+\left(\frac{2}{\xi}\right)\tilde{M}=0, \quad (31)$$

$$\frac{\partial\tilde{M}}{\partial\tau}+M_0\frac{\partial\tilde{M}}{\partial\xi}+\tilde{M}\frac{\partial M_0}{\partial\xi}=-\alpha\frac{\partial\tilde{\theta}}{\partial\xi}. \quad (32)$$

This is to note that there are only two physical variables $\tilde{\theta}(\xi)$ and $\tilde{M}(\xi)$, where $\tilde{g_s}(\xi)$ is limited up to the SSB only. Moreover, the external solar gravity affects only the equilibrium, and not the fluctuations. Quasi-linear coupling then provides a channel to solar-equilibrium control of the fluctuations. Now, carrying out the non-local linear plane-wave analysis, as outlined in the the SIP, we arrive at the following respective differential equations for the SWP fluctuations as

$$\left[\frac{\partial}{\partial\xi}+\frac{\partial\theta_0}{\partial\xi}+\left(ik+\frac{2}{\xi}\right)\right]\tilde{M}(\xi)=i\Omega\tilde{\theta}(\xi)-M_0\frac{\partial\tilde{\theta}(\xi)}{\partial\xi}, \quad (33)$$

$$\left[M_0\frac{\partial}{\partial\xi}-i\Omega+\frac{\partial M_0}{\partial\xi}\right]\tilde{M}(\xi)=-\alpha\left[\frac{\partial\tilde{\theta}(\xi)}{\partial\xi}+ik\tilde{\theta}(\xi)\right]. \quad (34)$$

We see that the operators come out to be the same as in equations (21)-(22). Now, allowing $\hat{O}_1$ to operate over equation (34) and $\hat{O}_2$ over equation (33), we derive two independent differential equations under $\hat{O}_1\hat{O}_2=\hat{O}_2\hat{O}_1$ as

$$a_0\frac{\partial^2\tilde{\theta}(\xi)}{\partial\xi^2}+b_0\frac{\partial\tilde{\theta}(\xi)}{\partial\xi}+c_0\tilde{\theta}(\xi)=0, \quad (35)$$

$$\frac{\partial M_0}{\partial\xi}\frac{\partial\tilde{M}(\xi)}{\partial\xi}+ik\frac{\partial M_0}{\partial\xi}\tilde{M}(\xi)+\frac{\partial^2M_0}{\partial\xi^2}\tilde{M}(\xi)=M_0\frac{\partial^2\theta_0}{\partial\xi^2}\tilde{M}(\xi)$$
$$-\left(\frac{2}{\xi^2}\right)M_0\tilde{M}(\xi), \quad (36)$$

where,

$$a_0=\left[\alpha-M_0^2\right],$$
$$b_0=\left[2i\Omega M_0-2M_0\frac{\partial M_0}{\partial\xi}+\alpha\frac{\partial\theta_0}{\partial\xi}+2\alpha\left(ik+\frac{1}{\xi}\right)\right],$$
$$c_0=\left[\Omega^2-k^2\alpha+ik\alpha\frac{\partial\theta_0}{\partial\xi}-ikM_0\frac{\partial M_0}{\partial\xi}+i\Omega\frac{\partial M_0}{\partial\xi}+\frac{2ik\alpha}{\xi}\right].$$

Now, as in the SIP, the lowest-order term in equation (35) when equated to zero, yields the dispersion relation as

$$\Omega^2-k^2\alpha+ik\alpha\frac{\partial\theta_0}{\partial\xi}-ikM_0\frac{\partial M_0}{\partial\xi}+i\Omega\frac{\partial M_0}{\partial\xi}+\frac{2ik\alpha}{\xi}=0. \quad (37)$$

Table 1. Initial and Boundary Values of Relevant Physical Parameters

Parameter	*Equilibrium*		*Fluctuation*	
	At ξ=0.01	*At* ξ=3.5	*At* ξ=0.01	*At* ξ=3.5
θ	$\theta = -10^{-3}$	$\theta = -1$	$\tilde{\theta} = -10^{-5}$	$\tilde{\theta} = -3\times10^{-4}$
	$\theta' = 0$	$\theta' = -0.62$	$\tilde{\theta}' = -10^{-6}$	$\tilde{\theta}' = -10^{-4}$
g_s	$g_s = \frac{1}{2}\xi_i e^{\theta}$	$g_s = 0.6$	$\tilde{g_s} = 10^{-4}$	N/A
	$g_s' = 0$	$g_s' = 0$	$\tilde{g_s}' = 2\times10^{-5}$	N/A
			$\tilde{g_s}'' = 10^{-5}$	N/A
M	$M = \frac{1}{2}\xi_i e^{\theta/2}$	$M = 10^{-7}$	$\tilde{M} = 10^{-11}$	$\tilde{M} = 5\times10^{-15}$
	$M' = -e^{\theta/2}$	$M' = 0$	$\tilde{M}' = 10^{-13}$	$\tilde{M}' = 0$

It is now simple to reduce equation (37) to a usual acoustic mode (p-mode) in uniform plasma background under the plane-geometry approximation ($\xi \to \infty$) as

$$\Omega^2 - k^2\alpha = 0. \tag{38}$$

This is clear that the analytic form of both the equations, (24) for the SIP and (36) for the SWP, is the same. Thus, the $\tilde{M}(\xi)$-profiles, on both the scales, are invariant under the applied operator commutator rule.

4 NUMERICAL ANALYSIS AND DISCUSSIONS

Before the numerical analysis, we apply the usual procedure of dynamical stability analysis (Dwivedi et al. 2007) to obtain a specific set of input and initial values of the relevant physical parameters. The initial and boundary values, thus obtained, are presented in Table 1.

4.1 SIP scale description and discussion of the fluctuations

We have used a numerical approach based on the incremental search method (Kiusalaas 2005) to solve the derived dispersion relation, equation (26), for the GES fluctuation description in the SIP. The obtained 3-D plots for real and imaginary parts of the frequency with variation in the k- and ξ- spaces are shown in Figs 4(a, b). The frequency plot in Fig. 4(a) depicts a specific domain in the k- space within $k = 10^{-4} - 0.8$ ($\lambda \approx 2\times10^4 - 2R_\Theta$), where the frequency is real with non-zero constant value. This is the same domain representing the usual Jeans mode with purely growing character. This is quasi-linearly transformed into an oscillatory mode, termed as the GES-oscillator. The more resolved Fig. 6(a) of the frequency plot depicts that this mode is localized within a domain of $k = 10^{-4} - 0.8$ ($\lambda \approx 2\times10^4 - 2R_\Theta$) in the k- space and $\xi \sim 1.5 - 3.5$ ($r = 0.4 - 1R_\Theta$ in the ξ- space. The limitation ($k\xi > 1$), imposed by the plane-wave approximation in the present analysis, makes the results in the core region, $\xi = 0 - 1.5$ ($r = 0.003 - 0.4R_\Theta$), unreliable.

Beyond the above mentioned domain in the k- space, the plasma GES-wave spectrum begins to exist. The growth rate is depicted in Fig. 4(b). The GES-oscillator is found to grow fast, whereas the GES-wave mode grows with a constant rate. Fig. 4(c) depicts the ratio of the real and imaginary parts of the frequency with variations in the k- and ξ- spaces. It is seen that the condition of the linear analysis ($\Omega_i/\Omega_r < 1$)

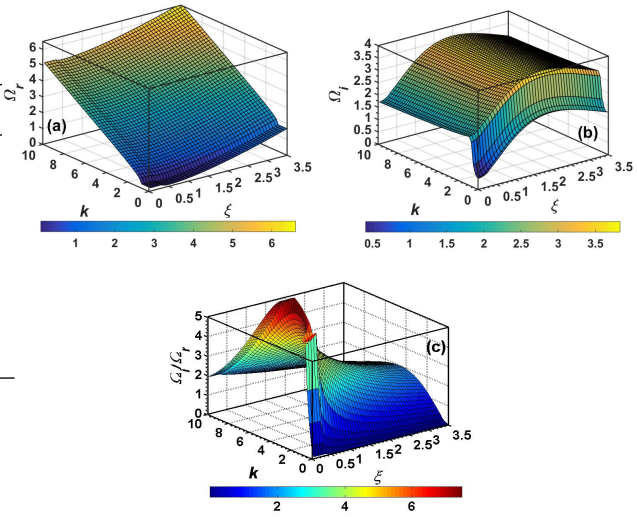

Figure 4. Profile of the normalized (a) real part (Ω_r), (b) imaginary part (Ω_i), and (c) imaginary-to-real part ratio (Ω_i/Ω_r) of the fluctuation frequency associated with the SIP flow dynamics with normalized position (ξ), and wave number (k). Different input and initial values used are described in Table 1 in the text.

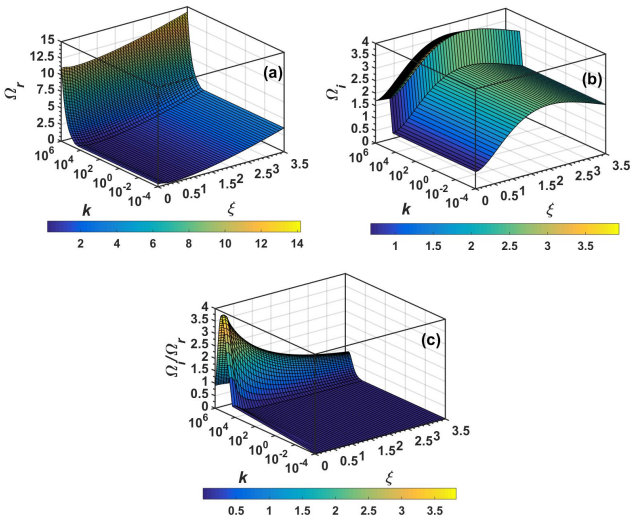

Figure 5. Same as Fig. 4, but in the extended k- space (high-k) on the logarithmic scale.

does not hold good in a wide-range domain of the k- and ξ- spaces and nonlinear analysis is the only remedy, which is for now, beyond the scope of the present work.

Fig. 5(a, b, c) depict the real and imaginary parts of frequency and the ratio of imaginary-to-real parts in the extended k-space to see the nature of natural modes in the high-k regions. It is seen that the frequency increases rapidly beyond the shorter wavelength range ($k \geq 10^4$, $\lambda \leq 190$ km).

In Figs 6(a, b), we depict the resolved real and imaginary frequencies in the lower range of the k- space ($k \sim 0-1$) to view the real nature of the GES-oscillator.

In Figs 7(a, b, c), we depict the phase velocity, group velocity and time period variations in the k- and ξ- spaces. The time period plot as shown in Fig. 7(c) depicts that the time

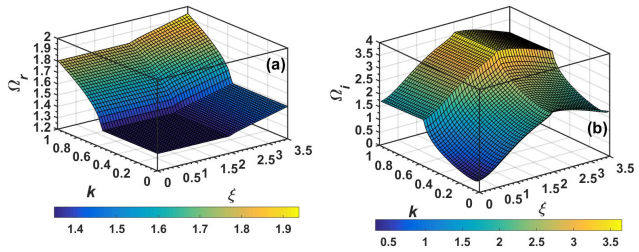

Figure 6. Profile of the normalized (a) real part (Ω_r), and (b) imaginary part (Ω_i) of the fluctuation frequency in the resolved k- space (low-k) of Fig. 4 associated with the SIP flow dynamics with normalized position (ξ). Different input and initial values used are the same as in Fig. 4.

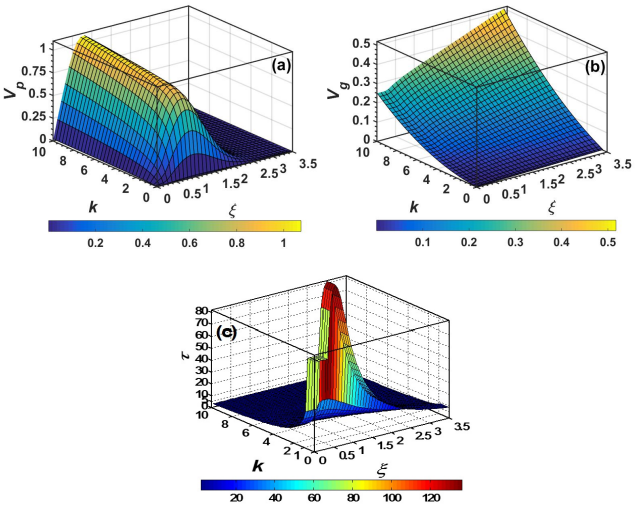

Figure 7. Profile of the normalized (a) phase velocity (V_p), (b) group velocity (V_g), and (c) unnormalized time period (τ) of the oscillations (in minute) associated with the SIP fluctuation dynamics with normalized position (ξ) and wave number (k). Different input and initial values used are the same as in Fig. 4.

periods of the GES-solar surface oscillations fall in the range of 3-10 minutes. From this plot, one can also see a small domain in the k- and ξ- spaces, where the GES-oscillator modes are found to have time period ranging between $\tau = 10 - 80$ minutes, but this is not reliable. These physical parameters in the extended space are shown in Figs 8(a, b, c). Interestingly, the oscillation period is found to be almost constant with three typical values of 3, 5 and 10 minutes period in three different zones of all the explored ranges of k at the SSB. The inset panel in Fig. 8(c) clearly shows the time period ($\tau = 10$ minutes) at the SSB for $k = 10^{-4} - 100$ ($\lambda \approx 2 \times 10^4 R_\Theta - 1.9 \times 10^4$ km) on the linear scale.

We have used the fourth-order Runge-Kutta (Kiusalaas 2005) method to solve the coupled ordinary differential equations [eqs (20), (24) and (25)] as an initial value problem to depict $\tilde{g_s}(\xi)$, $\tilde{\theta}(\xi)$ and $\tilde{M}(\xi)$ in the k- and ξ-spaces. Moreover, the inhomogeneous effects appearing in the form of the equilibrium parameters are properly included. The amplitude variations of $\tilde{g_s}(\xi)$, $\tilde{\theta}(\xi)$ and $\tilde{M}(\xi)$ in the k- and ξ-spaces are graphically depicted in Figs 9(a, b, c).

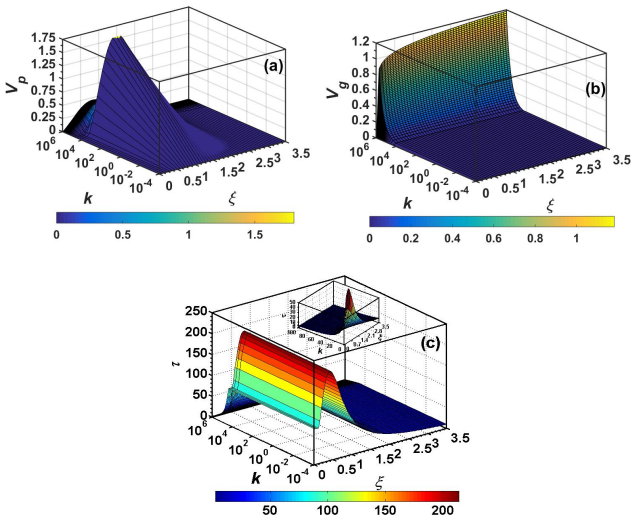

Figure 8. Same as Fig. 7, but in the extended k- space (high-k) on the logarithmic scale. The inset panel in Fig. 8(c) shows the time period on the linear scale as in Fig. 7(c).

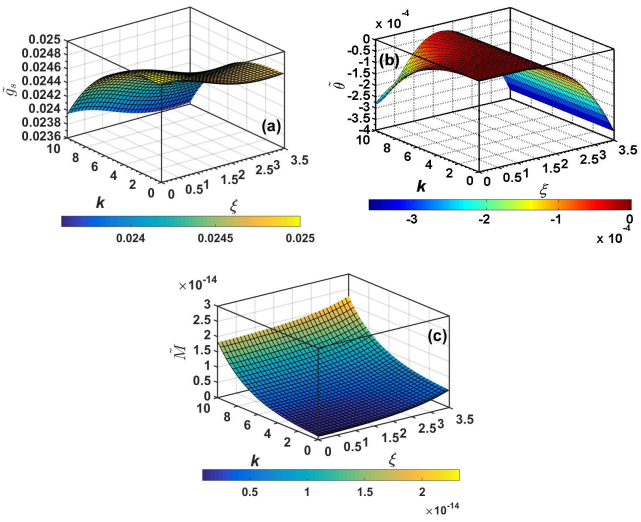

Figure 9. Profile of the normalized fluctuating (a) self-gravity [$\tilde{g_s}(\xi)$], (b) electrostatic potential [$\tilde{\theta}(\xi)$], and (c) Mach number [$\tilde{M}(\xi)$] associated with the SIP flow dynamics with normalized position (ξ) and wave number (k). Different input and initial values used are the same as in Fig. 1.

Numerically obtained profiles of amplitude variation for $\tilde{g_s}(\xi)$, $\tilde{\theta}(\xi)$ and $\tilde{M}(\xi)$ in the k- and ξ- spaces clearly imply that the self-solar gravity fluctuations dominate over the other two fluctuations by many orders of magnitude. The fluctuation level of $\tilde{g_s}(\xi)$ remains almost constant within order of magnitude in the ξ- space and falls down in the k-space. Furthermore, the form of the $\tilde{M}(\xi)$-profile [Fig. 9(c)] in the SIP is identical with that in the SWP [Fig. 16(b)].

In Figs 10(a, b, c), we depict the SIP fluctuation parameters [$\tilde{g_s}(\xi)$, $\tilde{\theta}(\xi)$ and $\tilde{M}(\xi)$] in the extended k- space. It is found that $\tilde{\theta}(\xi)$ dominates over the $\tilde{g_s}(\xi)$ for $k \geq 10^5$, which implies an interesting spectral mode transition from the gravito-electrostatic to pure electrostatic acoustic regimes.

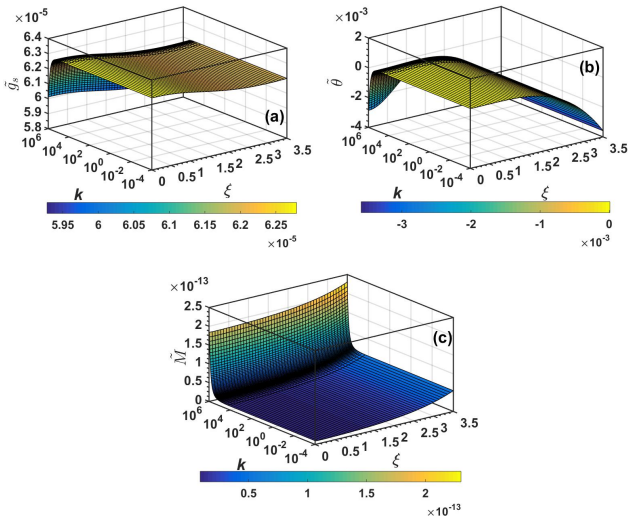

Figure 10. Same as Fig. 9, but in the extended k- space (high-k) on the logarithmic scale.

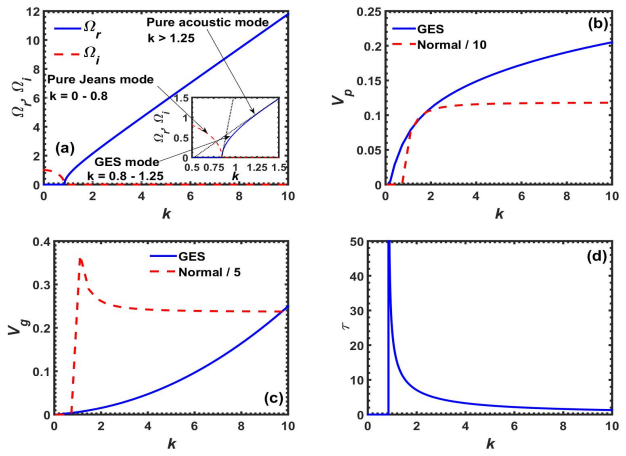

Figure 11. Profile of the normalized (a) real and imaginary parts of frequency (Ω_r, Ω_i), (b) phase velocity (V_P), (c) group velocity (V_g), and (d) unnormalized time period (τ) of the oscillations (in minute) associated with the SIP fluctuation dynamics with normalized wave number (k) for uniform planar plasma approximation. The significance of different lines is self-explanatory. Different input and initial values used are the same as in Fig. 4.

A set of Figs 11(a, b, c, d) are also constructed to depict the real and imaginary frequency parts of the usual Jeans dispersion relation along with the phase velocity, group velocity and time period for uniform plasma under the plane-geometry approximation. These plots should be helpful to understand the effect of non-uniform plasma background on the dispersion properties of the Jeans mode.

4.1.1 Salient features of the GES fluctuations

1. Logically speaking, the GES-oscillator mode is an outcome of the self-gravitational condensation, wherein, the infinitely longer wavelengths of the linear acoustic modes get condensed during the Jeans collapse itself. The condensation of the acoustic waves occurs through the cascading process, via which the long-wavelength wave energy gets transferred to shorter scales. Finally, the shortest possible wavelength is reached, where, the gravito-electrostatic coupling is maximum, as defined by $\alpha k^2 = 1$. From this condition, we find $k = 1/\sqrt{\alpha} \approx 0.8$, which in turn, results in $\lambda \sim 2R_\Theta$. Although, we start with $k = 10^{-4}$, but the frequency remains constant up to $k = 0.8$. At this specific k-value, both the GES-forces are in almost complete balance, and hence, the GES-Sun globally oscillates with the frequency decided by this k-value. Thus, the validity condition for the plane-wave analysis should be assessed for $k = 0.8$. The plane-wave approximation ($k\xi \geq 1$) will be satisfied in the radial domain, $\xi = 1.5 - 3.5$ ($r = 0.4 - 1R_\Theta$) only. It covers the radiative and convective zones in the standard terminology. The equilibrium inhomogeneity drives the GES-oscillator unstable.

2. The frequency of the GES-oscillator increases [Fig. 4(a)] in between $\xi = 1.5 - 3.5$. This is due to the increase of the restoring force produced by the electrostatic sheath-driven rebounding force as discussed earlier. The GES-oscillation mode causes the whole GES-Sun to oscillate globally with variable oscillation frequency in the ξ-space.

3. In the k-domain, $k = 0.8 - 100$ ($\lambda \approx 2.4\times10^6 - 1.9\times10^4$ km), the dispersive branch of the GES-wave mode exists [Fig. 8(a)]. The plane-wave approximation for these eigenmodes is ξ-dependent and all the wave-modes emanate with almost zero-velocity in the core. Then they propagate outward with increasing phase velocity, achieving supersonic speed of $v_p \approx 1.7c_S \sim 510$ km s^{-1} at $\xi = 1.5$ ($r = 0.4R_\Theta$), and thereafter, decreases almost to zero near the SSB.

4. In the k-domain, $k = 100 - 10^5$ ($\lambda \approx 1.9\times10^4 - 19$ km), the non-dispersive branch of the GES-wave modes exist [Fig. (8a)] in the entire SIP. For such modes, the plane-wave approximation will be valid in the entire solar interior. Thus, these waves can form the global standing wave-patterns.

5. In the k-domain, $k = 10^5 - 10^6$ ($\lambda \approx 19 - 1.9$ km), the usual p-mode exists, as is clear from Figs 10(a, b). These wave modes propagate independently without any hindrance from the proposed wall boundary of the GES-Sun. Such modes are weakly dispersive with phase velocity variation in the k- and in the localized ξ-domains with maximum $v_p = 510$ km s^{-1} at $\xi = 1.5$. At this location, the polarity of the net GES-force changes from negative to positive, and the curvature effect also loses its effective role to play.

6. In the domain, $k = 0.8 - 10^4$ ($\lambda \sim 2.4\times10^6 - 190$ km), the group velocity [Fig. (8b)] of the GES-wave modes remains sub-sonic in the whole SIP ξ-domain. Beyond this k-domain, the p-mode character dominates and its group velocity suffers a sudden increase to supersonic regime with maximum $v_g = 360$ km s^{-1} at the SSB for $k = 10^6$ ($\lambda \sim 1.9\times10^5$ cm).

7. Lastly, the oscillation time periods are in good agreement with the frequency profiles of our calculations. It is noted that the time periods for the entire calculated k-domains of the identified GES normal modes lie in the range of 3-10 minutes at the SSB, and interestingly, this matches with the observed ones (Christensen-Dalsgaard 2002; Alerts, Christensen-Dalsgaard & Kurtz 2010; Priest 2014)! Of course, the observed 5-minute peak is attributed to the usual p-mode with variation of the time period in between 3-10 minutes. This is not the case here, and the 5-minute oscillation links to the dispersive GES-wave mode!

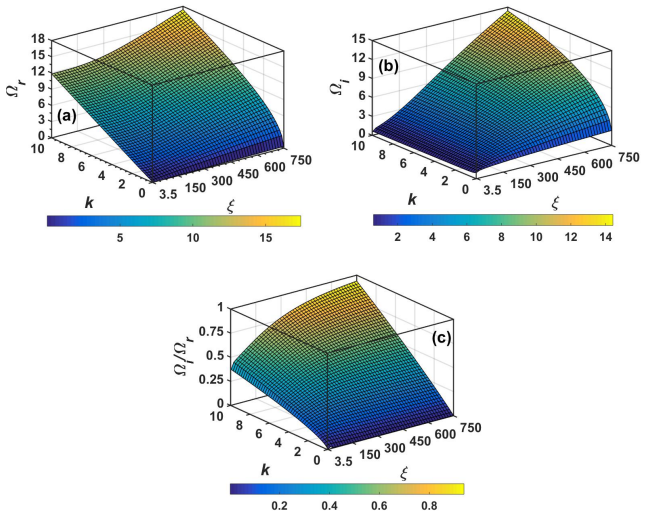

Figure 12. Profile of the normalized (a) real part (Ω_r), (b) imaginary part (Ω_i), and (c) imaginary-to-real part ratio (Ω_i/Ω_r) of the fluctuation frequency associated with the SWP flow dynamics with normalized position (ξ) and wave number (k). Details of input and initial values are presented in the text.

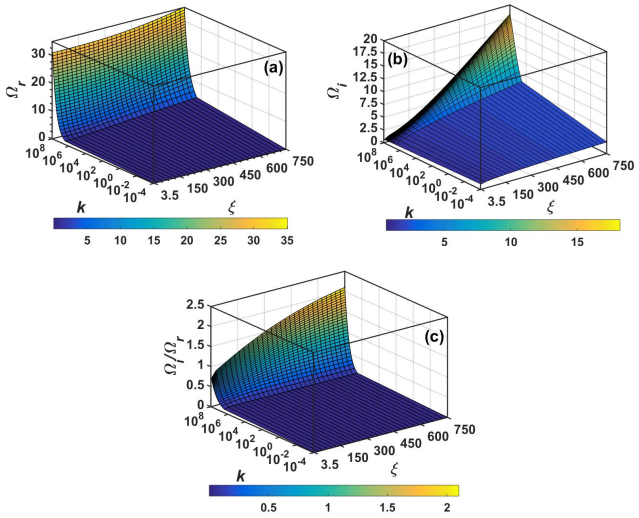

Figure 13. Same as Fig. 12, but in the extended k- space (high-k) on the logarithmic scale.

4.2 SWP scale description and discussion

We have used the same computational methods for evaluating the dispersion relation (eq. [37]) of the SWP fluctuations and their amplitude variations (eqs. [35] - [36]) as described before in subsection 4.1. In Figs 12(a, b, c), we depict the 3-D profiles of real and imaginary frequencies along with the ratio of the imaginary and real parts of the frequency in the numerically explored k-domain of $k = 10^{-4}-10$ ($\lambda \approx 2\times10^{4}-0.2R_{\Theta}$) and ξ- space of $\xi = 3.5-750$ ($r = 1-215R_{\Theta}$). Here, $r = 750\lambda_J = 1$ A.U. defines the mean distance from the Sun to the Earth. The 3-D profiles of the phase velocity, group velocity and time period of the SWP fluctuations in the same k- and ξ-spaces are portrayed in Figs 14(a, b, c). Lastly, Figs 16(a, b) describe the 3-D profiles of $\tilde{\theta}(\xi)$ and $\tilde{M}(\xi)$ in the same k- and ξ- spaces.

The dispersion characteristic features of the SWP fluctuations, as shown in Figs 12(a, b, c), clearly match with that of the well-known plasma acoustic mode. Weak dispersion is noted in a short range of $k = 10^{-4} - 4$ ($\lambda \approx 2 \times 10^{4} - 0.5R_{\Theta}$) in the inhomogeneous plasma medium that persists up to $r = 750\lambda_J = 1$ A.U. The equilibrium non-uniformity in the SWP flow and the electrostatic sheath potential are found to act respectively as a free source of *kinetic* and *potential* energies to drive the acoustic mode unstable. The effect of geometry, i.e., deviation from plane-geometry approximation appears to suppress the instability. However, as a whole, the sound mode is unstable in the SWP. The linear theory (validated by $\Omega_i/\Omega_r < 1$) is effective within a reasonable domain of the explored k- and ξ-spaces [Fig. 12(c)].

Figs 13(a, b, c) display the above dispersion properties in the extended space of $k = 10^{-4} - 10^{8}$ ($\lambda \approx 2 \times 10^{4} - 2 \times 10^{-8}R_{\Theta}$). Like in the SIP, the SWP fluctuation frequency increases towards the shorter wavelength (few hundred meters) thereby exhibiting analogous dispersive mode features and becoming almost constant in the k-space.

The propagation speeds (phase and group velocities) in the range of $k = 10^{-4} - 10$ and $\xi = 3.5 - 750$ are displayed in Figs 14(a, b). From Fig. 14(a), it looks, as if, the acoustic modes are divided into two groups as follows.

The first group of waves, which looks dispersive in nature, is localized in the domain, $k = 10^{-4} - 6$ ($\lambda \approx 2\times10^{4} - 0.75R_{\Theta}$). The phase velocity of this group increases radially outwards and acquires supersonic value with subsonic transition beyond about $k = 6$. The second group of waves, which is almost non-dispersive in nature within a wide-range of the ξ-space, is localized in a wide-range of k-domain [Fig. 14(a) and Fig. 15(a)]. The propensity of weak dispersion is reflected near the SSB. These waves are found to travel within sub-sonic range of flow speed. From Fig. 14(b), it is clear that the group velocity is almost constant in the k-space. Moreover, no distinction is noted between the two groups. However, the group velocity increases radially outwards with the asymptotic sonic speed value at 1 A.U.

In Fig. 14(c), we depict the time period plot in the k- and ξ-spaces. The categorization of the two distinct groups of waves is clearly visible. The time periods of the dispersive mode group are found to be larger than those of the non-dispersive wave group, but at different ξ. It also reveals that discreteness in the low k-value of the fluctuations results in discreteness in the oscillation period peaks. In the range of relatively high k-value and beyond, such discrete peaks in the oscillation period are not observed.

In Figs 15(a, b, c), we depict the phase velocity, group velocity and time period in the extended k-space. Also, the time period decreases towards shorter wavelength. Figs 16(a, b) depict that the electrostatic potential fluctuation level, being higher, dominates over the SWP flow fluctuations. One more thing, to say, is that the amplitude profile of the flow fluctuations is the same as that of the SIP.

Finally, Figs 17(a, b) show the SWP fluctuation parameters [$\tilde{\theta}(\xi)$ and $\tilde{M}(\xi)$] in the extended k-space. The electrostatic potential fluctuations increase towards the shorter wavelength regime. The flow fluctuations are not affected much in the shorter wavelengths. This is in conformity with

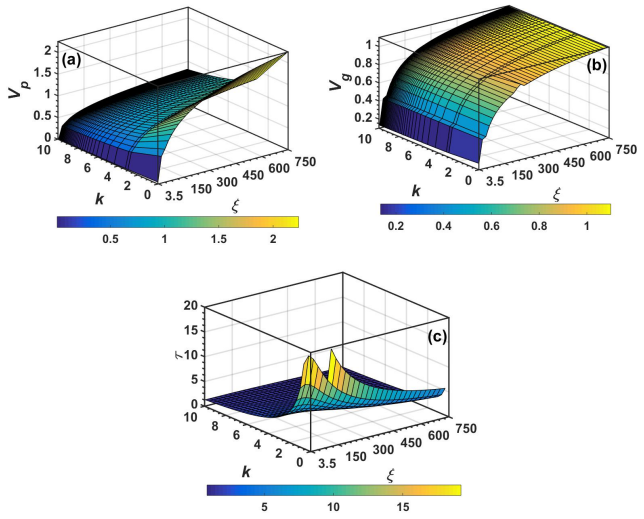

Figure 14. Profile of the normalized (a) phase velocity (V_p), (b) group velocity (V_g), and (c) unnormalized time period (τ) of the oscillations (in minute) associated with the SWP fluctuation dynamics with normalized position (ξ) and wave number (k). Different input and initial values used are the same as in Fig. 12. In Fig. 14(c), discreteness in the low k-value results in the τ-discreteness as period peaks.

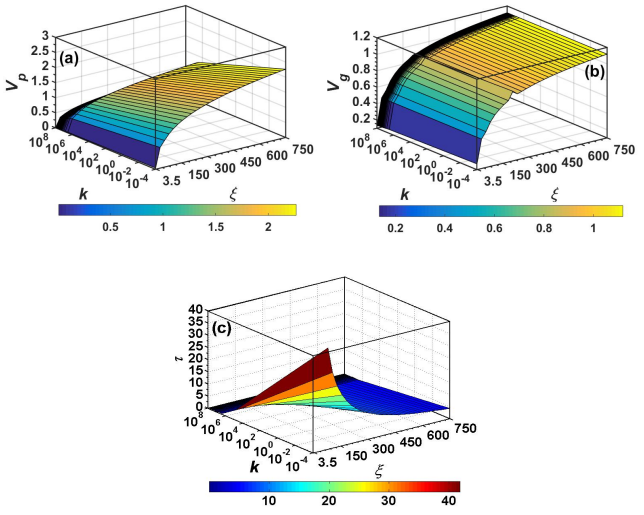

Figure 15. Same as Fig. 14, but in the extended k- space (high-k) on the logarithmic scale.

the flow-pattern phenomena as observed in the SIP as well. Some specific features in addition, are enlisted as below.

1. The phase velocity of the non-dispersive p-modes, as identified and discussed above in Fig. 14(a)-15(a), varies in the sub-sonic range only. But, that of the dispersive branch of the p-modes, varies from sub-sonic to supersonic regime with maximum $v_p \sim 200$ km s^{-1} at 1 A.U.

2. The phase velocity plot in the extended k-domain [Fig. 15(a)] exhibits a similar type of behavior of sub-sonic and supersonic speeds. The corresponding group velocity [Fig. 14(b) and Fig. 15(b)] acquires sonic speed, $v_g \approx 100$ km s^{-1}, at 1 A.U in all the k-domains.

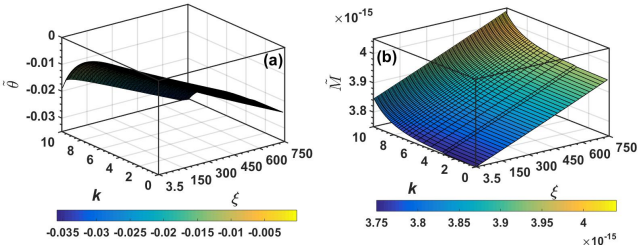

Figure 16. Profile of the normalized fluctuating (a) electrostatic potential [$\tilde{\theta}(\xi)$], and (b) Mach number [$\tilde{M}(\xi)$] associated with the SWP flow dynamics with normalized position (ξ) and wave number (k). Different input and initial values are as in Fig. 12.

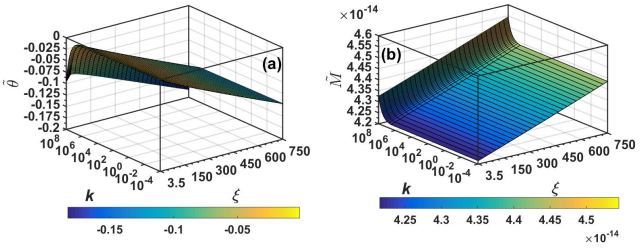

Figure 17. Same as Fig. 16, but in the extended k- space (high-k) on the logarithmic scale.

3. The time period plots [Fig. 14(c) and Fig. 15(c)] exhibit strong radial dependence with two distinct peaks, $\tau \approx 20$ minutes each, lying at $\xi \approx 30$ ($r = 30\lambda_J \approx 10R_\Theta$ away from the SSB) and $\xi \approx 130$ ($r = 130\lambda_J \approx 37R_\Theta$). The time period varies in between $\tau = 1 - 5$ minutes at 1 A.U.

4. From Fig. 13(a) of the frequency plots in an extended k-domain, one can notice that the frequency suddenly increases to quite large value of $\Omega_r = 30 - 35$ ($\Omega_{phys} = 30 - 35\omega_J$) in the k-range within $k = 10^6 - 10^8$ ($\lambda \approx 2$ km - 20 m) of the acoustic wavelength. From Fig. 15(a), one can notice that the phase velocity decreases to sub-sonic values towards the shorter wavelengths. The group velocity exhibits sonic transition at about $\xi = 450$ ($r = 450\lambda_J \approx 130R_\Theta$) and achieves maximum value of $v_g \approx 100$ km s^{-1} at 1 A.U.

5. It is now clear that the phase velocity variation from the SSB to 1 A.U. ranges in between about $v_p = 10 - 200$ km s^{-1}. Recently, Vranjes (2011) studied the EIT waves [named after the Extreme-ultraviolet Imaging Telescope (EIT), onboard the SOlar and Heliospheric Observatory (SOHO)]. These are described in the literature as Fast Magneto-Acoustic (FMA) modes. However, the observations show that a large percentage of these events propagate with very small speeds, that may be as low as 20 km s^{-1}. This is far below the FMA wave speed which cannot be below the sound phase speed, the latter being typically larger than 100 km s^{-1} in the corona. Then, the idea of internal gravity modes is provoked to explain these events. Nevertheless, our model calculations demonstrate the possibility of the low-phase velocity acoustic modes. Thus, even without invoking the idea of internal gravity modes, the observed phase velocity range for the EIT waves can be explained in terms of the p-modes!

5 COMMENTS AND CONCLUSIONS

5.1 Brief comments

It is recognized that the findings of our non-local linear perturbation analysis for the GES fluctuations springs up as a first approximation. Our theoretical-cum-computational approach for non-local linear perturbation analysis is general in nature, and consistently, accounts for any arbitrary inhomogeneity in the background plasma equilibrium. We recognize that the plane-wave approximation becomes invalid in the core region ($\xi \leq 1.5$) of the GES-Sun in certain domain of the k-space as discussed in the text. Probably, the consideration of spherical wave may be required to describe the proper nature of collective plasma dynamics, specifically, within the core region. To improve the present perturbational analysis to incorporate the effect of inhomogeneity on the wave vector, a better approach based on the quasi-classic WKB or eikonal methods (Elmore 1969; Ostashev & Wilson 2016) would be needed. These methods could be useful to find out analytical solution of the GES wave fluctuation level. The effect of magnetic field on the GES equilibrium and fluctuations could be included within the framework of the Chodura sheath formalism with proper care of geometrical boundary.

5.2 Conclusions

Based on our theoretical and numerical analyses in detail, we identify three distinct branches of the radial GES natural normal modes as described below.

1. *GES-oscillator*-This mode is purely oscillatory in nature and has finite linear temporal growth. It is localized in the k- space ($k = 10^{-4} - 0.8$, $\lambda \approx 2\times10^4 - 2R_\Theta$) and globalized in the ξ- space with constant oscillator frequency ($\Omega_r = 1.2$) up to a radial point, $\xi = 3$. Beyond it, the frequency increases linearly up to $\Omega_r = 1.5$ at $\xi = 3.5$, which defines the radial position of the GES-SSB. Its time period is $\tau \approx 10$ minutes at the solar surface for all $k = 10^{-4} - 0.8$. Its origin and physics could be understood in terms of the initial scenario of the Jeans collapse of self-gravitating matter fluids.

Let us argue that the long-wavelength acoustic perturbations condense along with the collapse as because these waves cannot move away from the collapsing mass. As time progresses, the acoustic waves in the collapsing plasma medium will change and readjust in the presence of time-varying equilibrium inhomogeneity till the collapse is arrested thereby establishing a new equilibrium configuration. In the final stage, the long-wavelength wave energy will be transferred to the shorter ones till the gravito-electrostatic sheath coupling becomes maximum at some specific value of $k = 0.8$ ($\lambda \approx 2.4 \times 10^6$ km $\approx 2R_\Theta$).

The constant oscillator frequency in the specified k-domain ($k = 10^{-4} - 0.8$) implicates that the constant frequency corresponds to the trapping of only one particular acoustic wavelength within the SIP causing thereby the global surface oscillations observable at the SSB. In other words, we can say that the whole global wall oscillates like swelling and contraction of the SSB. The *self-solar gravitational wall-produced electrostatic sheath force field*, which we call as the electrostatic *sheath rebounding force*, acts as a restoring force field to drive the GES-oscillator.

Quasi-linear effect, i.e., *coupling of the equilibrium with linear normal modes* acts as a source; and the curvature effect, as the sink. The linear growth of the oscillator amplitude implies that the source is dominating over the sink, and hence, the GES-oscillator mode is driven unstable. This is unique in nature and different from the other known modes, like g-mode, gravito-acoustic mode, etc. Dispersion relations of these familiar modes have been derived and well-studied under constant-gravity approximation in the literature (Leighton, Noyes & Simon 1962; Frazier 1968a,b; Ulrich 1970; Leibacher & Stein 1971; Deubner 1975; Christensen-Dalsgaard & Gough 1976). In fact, the self-solar gravitational fluctuations are the property of the Jeans mode, which convert themselves self-consistently by acoustic trapping process into the GES-oscillator mode.

2. *GES-wave* - Its fluctuating features are the same as those of the GES-oscillator, but it has propagatory character, too. All the GES-waves start propagating with zero-phase velocity and acquire some maximum value of sonic speed-order at around $r = 1\lambda_J = 0.3R_\Theta$, as discussed in the text. Finally, the phase velocity again terminates into almost the zero-level near the defined gravitational sheath boundary located at $\xi = 3.5$ ($r = 1R_\Theta$). This wave mode exists over a wide-range of k-domains within $k = 0.8 - 10^5$ ($\lambda \approx 2.4\times10^6 - 19$ km). Typical time period of the dispersive GES-wave ($k = 0.8 - 4$, $\lambda \approx 2.4\times10^6 - 5\times10^5$ km) at the SSB is $\tau = 5$ minutes and that of the non-dispersive GES-waves ($k = 4 - 10^5$, $\lambda = 5 \times 10^5 - 19$ km) is $\tau \approx 3$ minutes. This mode is also different from the usual gravito-acoustic modes existing in the literature.

3. *Electrostatic acoustic wave* - For the larger values of $k = 10^5 - 10^6$ ($\lambda = 19 - 1.9$ km), the self-solar gravity fluctuation levels are quite reduced and are eventually converted into electrostatic fluctuations called as the usual p-modes.

These normal modes are linearly unstable, and hence, can drive the nonlinear turbulence which is a quite important subject for astrophysical problems. It is beyond the scope of our present study. According to our model approach, the solar surface oscillations should consist of the GES fluctuations as an intrinsic property. The SWP fluctuations are of pure plasma acoustic mode in origin, that is, the p-modes in conventional helioseismic terminology. Consideration of spherical harmonics is the only remedy for depicting the core plasma dynamics, which may be quite complicated to handle, theoretically as well as numerically. We would like to comment that the experimental measurements of the *self-solar gravity fluctuations* will be required to ascertain the reality of these GES-associated modes.

5.3 Future scopes

Further improvements and necessary refinements of the GES-theory for both the equilibrium as well as the fluctuations are to be implemented so as to make it more realistic. Our proposed GES model offers a wide scope of future interdisciplinary research work for Plasma Physicists and Astrophysicists both. Nevertheless, we would like to pinpoint a couple of research problems to be undertaken in imminent course of our study.

1. It is intuitively felt that relaxing the constant temperature approximation, and by using the energy transport equation invoking thermal energy minimization for the SIP

and SWP both; the solar chromospheric *T-valley* problem is likely to be resolved under the proposed GES model.

2. Study of parametric coupling of the GES-oscillator with the SWP bulk acoustic modes forms another interesting problem in astrophysical plasmas. This may give the possible signatures of the GES effect on the SWP mode at heliosesmic distances.

ACKNOWLEDGEMENTS

We acknowledge the Dr. K. S. Krishnan Geomagnetic Research Laboratory, Allahabad, for interaction facility. The Department of Science and Technology (DST), New Delhi, for the SERB Fast Track Project (Grant No. SR/FTP/PS-021/2011), is duly recognized. Finally, we acknowledge the anonymous referees' contribution to quality improvement through insightful comments and suggestions.

REFERENCES

Alerts C., Christensen-Dalsgaard J., Kurtz D. W., 2010, Asteroseismology. Springer, Berlin
Bellan P. M., 2004, Fundamentals of plasma physics. Cambridge University Press, cambridge
Chen F. F., 1984, Introduction to plasma physics and controlled fusion. Plenum Press, New York
Chodura R., 1982, Phys. Plasmas, 25, 1628
Christensen-Dalsgaard J., Gough D. O., 1976, Nature, 259, 89
Christensen-Dalsgaard J., 2002, Rev. Mod. Phys., 74, 1073
Cowling T. G., 1941, MNRAS, 101, 367
Deka U., Dwivedi C. B., 2010, Braz. J. Phys., 40, 333
Deubner F. L. 1975, A & A, 44, 371
Dwivedi C. B., Karmakar P. K., Tripathy S. C., 2007, ApJ, 663, 1340
Elmore W. C., Heald M. A., 1969, Physics of waves. Dover Publications, Inc., New York
Frazier E. N., 1968a, ApJ, 152, 557
Frazier E. N., 1968b, Z. Astrophys., 68, 345
Jeans J. H., 1902, Phil. Trans. Roy. Soc., 199, 1
Karmakar P. K., Dwivedi C. B., 2011, Int. J. Astron. Astrophys., 1, 210
Kiusalaas J., 2005, Numerical methods in engineering with MATLAB. Cambridge University Press, Cambridge
Leibacher J. W., Stein R. F., 1971, ApJ, 7, 191L
Leighton R. B., Noyes R. W., Simon G. W., 1962, ApJ, 135, 474
Loizu J., Ricci P., Theiler C., 2011, Phys. Rev. E, 83, 016406
Ostashev V. E., Wilson, D. K., 2016, Acoustics in moving inhomogeneous media. Taylor & Francis, London
Pandey B. P., Avinash K., Dwivedi C. B., 1994, Phys. Rev. E, 49, 5599
Pandey B. P., Vladimirov S. V., 2011, EPL, 94, 55002
Parker E. N., 1958, ApJ, 128, 666
Peratt A. L., 2015, Physics of the plasma universe. Springer, New York
Pines V., Zlatkowski V., Chait A., 2010, Adv. Space Res., 46, 942
Priest E., 2014, Magnetohydrodynamics of the Sun. Cambridge University Press, Cambridge
Riemann K. U., 1991, J. Phys. D, 4, 493
Riemann K. U., 1997, Phys. Plasmas, 4, 866
Stix M., 2002, The Sun: An introduction. Springer, Berlin
Ulrich R. K., 1970, ApJ, 162, 993
Vranjes J., 2011, Phys. Plasmas, 18, 062902

APPENDIX A: PROOF FOR CHARGE-CONSERVATION PRINCIPLE

Under the Boltzmannian electron density distribution, the electron continuity equation becomes redundant as because the basic set of equations (eqs. [1], [2] & [4]) forms a closed set. However, we will use it to estimate the electron current flowing across the spherical concentric surfaces at varying radial positions relative to the helio-center. Thus, one can write the normalized form of the total electron flux conservation in spherical geometry with conventional notations as

$$N_e(\xi)V_e(\xi)\xi^2 = N_{ei}V_{ei}\xi_i^2. \tag{A1}$$

Let us now consider V_{ei} as the initial equilibrium electron velocity, equal to the Maxwell-Boltzmannian mean thermal velocity, $V_{ei} = (m_i/m_e)^{1/2}e^{\theta}$, as derived and discussed by kinetic approach in the context of the plasma sheath physics and probe theory (Bellan 2004, Ch. 2). Now, the normalized form of the electron current density can be expressed as

$$J_e = -N_e(\xi)V_e(\xi) = -N_{ei}\left(\frac{m_i}{m_e}\right)^{1/2}\left(\frac{\xi_i}{\xi}\right)^2 e^{\theta}. \tag{A2}$$

The role of spherical geometry in electron flux density variation now appears in this expression (eq. [A2]), which was indeed missing in our earlier expression. So, the present form offers a correction to the earlier one (Dwivedi et al. 2007; Karmakar & Dwivedi 2011). The normalized ion current density due to inertial motion of the ions is now given as

$$J_i = M. \tag{A3}$$

The net current density, J, flowing across the spherical surfaces of the GES plasma can be expressed as

$$J = J_i + J_e = M - \left(\frac{m_i}{m_e}\right)^{1/2}\left(\frac{\xi_i}{\xi}\right)^2 e^{\theta}, \tag{A4}$$

where, the normalized initial densities, $N_{ei} = N_{ii} = N_i = 1$ at $\xi = \xi_i$. The first term in equation (A4) corresponds to the inertial flow velocity produced by gravito-electrostatic sheath forces, which is written in splitted form in our previous publication (eq. [26] in Dwivedi et al. 2007). The second term in equation (A4) arises due to exponential electron current as discussed and estimated in the case of the basic sheath physics and probe theory (Bellan 2004). As a consequence, in the steady-state, the charge conservation equation in spherically symmetric geometry is expressed as

$$\frac{\partial J}{\partial \xi} + \left(\frac{2}{\xi}\right)J = 0. \tag{A5}$$

This is obtained by combining the electron and ion continuity equations in spherically symmetric geometry. This equation (eq. [A5]) has been solved numerically using the expression of the net current density (eq. [A4]) and the plots are shown in Figs. 1(f) & 2(f). The net current density profile in the SIP, as shown in Fig. 1(f), differs from that shown in Fig. 4(a) of Karmakar & Dwivedi (2011). This difference could be attributed to the present consideration of the role of geometry in the calculation scheme of the electron thermal flux (eqs [A1]-[A2]). The SWP current profile is not much affected as shown in Fig. 2(f). The charge conservation equation (eq. [A5]) is well-satisfied both in the SIP as

well as SWP for the net current density given in equation (A4) as shown in Figs. 1(f) & 2(f).

It is, thus, inferred that a finite non-zero current, with sign reversal beyond the SSB, does indeed exist under the plasma sheath formalism of the Sun without violating the basic charge conservation principle.